POLITECNICO DI TORINO
Repository ISTITUZIONALE

On the Pyroelectric and Triboelectric Phenomena in Ferrofluids

Original
On the Pyroelectric and Triboelectric Phenomena in Ferrofluids / Garofalo, E., Bevione, M., Cecchini, L., Chiolerio, A.. - In: ADVANCED MATERIALS TECHNOLOGIES. - ISSN 2365-709X. - ELETTRONICO. - (2022), p. 2200127. [10.1002/admt.202200127]

Availability:
This version is available at: 11583/2964833 since: 2022-05-27T16:58:39Z

Publisher:
John Wiley and Sons Inc

Published
DOI:10.1002/admt.202200127

Terms of use:

This article is made available under terms and conditions as specified in the corresponding bibliographic description in the repository

Publisher copyright

(Article begins on next page)

19 November 2026

Check for updates

ADVANCED MATERIALS TECHNOLOGIES
www.advmattechnol.de

On the Pyroelectric and Triboelectric Phenomena in Ferrofluids

*Erik Garofalo, Matteo Bevione, Luca Cecchini, and Alessandro Chiolerio**

Owing to the waste of energy originated by any physical or chemical process, approaches for reducing the energy losses have been conceived and, nowadays, energy recovery and conversion systems represent a worldwide-recognized solution. The advent of colloidal-based cybernetic systems highlights the essential role of energy harvesting, storage, and management capabilities coped by colloidal energetic systems. In this work, an alternative to thermoelectricity generation is demonstrated by means of a magnetic colloid based on Fe_3O_4 nanoparticles (NPs). The ferrofluid (FF) tribo- and pyroelectric features are explored in order to increase the amount of harvested energy. The findings suggest that the FF shows both triboelectric and pyroelectric charge displacement. A capacitive electrode is more efficient for accumulating potentials up to 48 V developed by triboelectricity while a resistive one is essential to collect pyroelectric charges up to 22 nA, which helped to estimate the FF pyroelectric coefficient, reaching the remarkable value of 25.2 $\mu Cm^{-2} K^{-1}$. A simplified equivalent model of the inductive setup is proposed, suggesting that increasing the fluid temperature a reduction of FF inductance due to demagnetization effects occurs.

1. Introduction

Energy is what powers any anthropic, biological, and artificial process, at all levels. The energy produced for heating a material, moving an object or powering an electronic device is always higher than the energy effectively absorbed by the process: this is what the second law of thermodynamics states. A reason must be sought in the irreversible nature of any thermodynamic transformation. As consequence, energy is always wasted in a quantity that strictly depends on the physical or chemical processes governing the system and, usually, in the form of thermal dispersions, mechanical vibrations, and electromagnetic radiations. Several approaches for reducing energy losses have been conceived and, nowadays, many energy recovery, harvesting, and conversion systems are investigated, many of them being already available on the market. Energy harvesting is defined as the process wherein the sources such as mechanical load, vibrations, temperature gradients, heat, light, salinity gradients, and wind are scavenged and converted to obtain relatively small levels of power in the nW–mW range.[1] According to the field of interest, energy-harvesting systems differ in the working principles and the employed materials, as a direct consequence of the physical effects exploited for the energy conversion. For example, in the industrial, domestic, and automotive applications, the thermoelectric generators (TEGs) are widely used, while in the wearable and Internet of Things (IoT) sectors, piezoelectric, pyroelectric and triboelectric devices find their space.[2] More recently, in order to increase the energy efficiency and the autonomy level of intelligent robots, harvesting energy from the external environment and internal subsystems has become fundamental.[3–5] In particular, with the advent of soft robots, composed of highly compliant materials similar to those found in living organisms,[6] energy harvesting from many sources has been explored, mainly for mobility purposes.[7,8]

Advancements of materials science and cybernetic systems technology in the field of Smart Fluid Systems (SFS) show that, compared to conventional robotic systems, colloid-based robots offer advantages in versatility, adaptability, resiliency, distributed architecture, and autonomy especially for applications in harsh environments, both space and terrestrial.[9] Colloidal devices at the liquid state represent a new paradigm in the field of cybernetic systems, joining the versatility of conventional robotics and the advantages of soft robotics. Here, energy harvesting, storage, and management capabilities cover an essential role.[10] For this purpose, the engineering feasibility of an energy harvesting and storage system applicable to SFS, named Colloidal EneRgEtic System (CERES), has been assessed.[10] Colloids are complex condensed matter agents lying at the boundary between completely homogeneous systems such as solutions and completely

E. Garofalo
Istituto Italiano di Tecnologia
Center for Sustainable Future Technologies
Via Livorno, 60, Torino 10144, Italy
E. Garofalo
Department of Electronics and Telecommunications
Politecnico di Torino
Corso Duca degli Abruzzi, 24, Torino 10129, Italy
M. Bevione, L. Cecchini, A. Chiolerio
Center for Sustainable Future Technologies
Istituto Italiano di Tecnologia
Via Livorno, 60, Torino 10144, Italy
E-mail: alessandro.chiolerio@iit.it
L. Cecchini, A. Chiolerio
Bioinspired Soft Robotics Laboratory
Istituto Italiano di Tecnologia
Via Morego, 30, Genova 16163, Italy
The ORCID identification number(s) for the author(s) of this article can be found under https://doi.org/10.1002/admt.202200127.

© 2022 The Authors. Advanced Materials Technologies published by Wiley-VCH GmbH. This is an open access article under the terms of the Creative Commons Attribution-NonCommercial License, which permits use, distribution and reproduction in any medium, provided the original work is properly cited and is not used for commercial purposes.

DOI: 10.1002/admt.202200127

heterogeneous systems such as suspensions.[9] They are defined as stable dispersions of nanoparticles (NPs) in a carrier fluid, in liquid or gaseous form, and they are classified according to the aggregation state of their components. The employment of colloids for energy harvesting purposes is a relatively new research field, where the capability of triboelectric[11] and pyroelectric[12] colloids has been validated for the scopes of converting thermal energy into electrical power. In particular, magnetic colloids, such as ferrofluids (FFs), are nanomaterials that present high magnetic susceptibility[13] and whose flow and energy transport processes can be influenced and controlled by adjusting the strength and orientation of an external magnetic field.[14] For these reasons, FFs are promising materials for in situ sensing, mobility, energy storage, harvesting, and conversion, giving the possibility to develop ultralow-power micro harvesters with very high thermal conductivity and capacity, well suited for high temperature heat flux applications, such as in oscillating heat pipes[15] and ThermO-magnetic hydRO-DYNAmic energy harvesting (TORODYNA) systems.[16]

In this work, we demonstrate an alternative thermoelectricity generation by means of FFs, whose implications may bring future developments of cybernetic system, industrial, automotive, and domestic energy harvesters. The FF selected for the experiments is a light hydrocarbon oil-based suspension of magnetite (Fe_3O_4) NPs. Considering the liquid nature of the colloid, any heat flux coming from different waste heat sources, can trigger the convection motion of the fluid. Once the fluid is moving, two different physical effects can be exploited which are strictly dependent on the dynamics of the colloid: the electromagnetic induction, thanks to magnetic properties of FF, and the triboelectrification, considering the electronic exchange between the colloid and the channel through which it is moving. Furthermore, since the fluid is heated, it experiences a thermal gradient, both spatial and temporal, that generates charges accumulation on the colloid NPs thanks to its pyroelectric properties. Since heat fluxes can take different forms such as solar radiation, hot bodies, and heated fluid streams, in this work we generalized the heat source and the consequent motion, governed by natural or Rayleigh–Bénard convection processes,[17] by using a lab heater and a peristaltic pump, respectively. In this way, the pump simulates the effect of a common convective motion at different temperature level thanks to the heating plate.

2. Results and Discussion

2.1. Investigation of Inductive, Pyroelectric, and Triboelectric Phenomena

First, we explored the capability of FF of inducing electromotive force when flowing through an inductive electrode. We tested three different Fe_3O_4 volumetric concentrations (2%, 4%, and 6%) in order to encompass a broader range of Magnetic Reynolds number, setting the flow speed from 0 to 5 cm s^{-1}, respectively 0 and 10 arbitrary unit (A.U.). Surprisingly, **Figure 1** shows that, when the concentration of Fe_3O_4 NPs in the FF is lower, the recorded potentials and currents are higher (60 μV and 7 μA) showing an increasing trend as a function of velocity. The unfavorable magneto-viscous negative effects in correspondence of the inductive electrode offer an explanation to the less impacting harvesting efficiency for higher solid volumes. This is the reason why in the following experiments we exploited FFs with a concentration of Fe_3O_4 NPs equal to 2% vol. (referred to as 2% FF). In this case (Figure 1a), the potential increases with the velocity except in correspondence of 6 A.U. when, likely, the transition of boundary layer in the pipe from laminar to turbulent generates high disturbance that, in turns, negatively affects the inductive performance of FF. Alternatively, the flow at 6 A.U. could be chocked. Consequently, a downstream shock wave occurs reducing the inductive performance. In fact, the recorded potential returns and saturates at the previous value (related to velocity equal to 4 A.U.), even if the velocity is further increased.

Subsequently we analyzed the potentials and currents generated on the capacitive electrode at different flows velocities in a range far from saturation (we used A.U. so that: V1 = 0.22 mm s^{-1}, V2 = 0.44 mm s^{-1}, V3 = 0.66 mm s^{-1}, V5 = 1.1 mm s^{-1}, V10 = 2.2 mm s^{-1}). **Figure 2** shows increasing potentials and currents with increasing speed to a maximum of about 48 V and 2.8 nA.

Finally, we examined the contribution of the charges displaced by means of the pyroelectric effect when the colloid is heated and, flowing through the pipe, it comes into contact with the resistive electrodes. We measured both potentials and currents as a function of the fluid velocity when the recorded temperature in the beaker was 60 °C and we compared the values with the case when the colloid was flowing at room

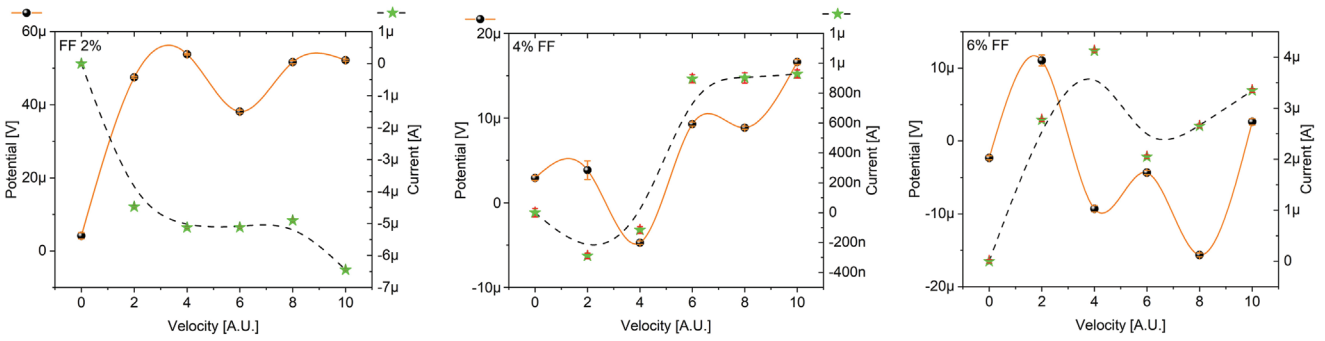


Figure 1. Comparison between harvested potentials and currents by means of the inductive electrode for ferrofluids (FFs) featuring increasing volume concentration (2%, 4%, and 6%) of Fe_3O_4.

© 2022 The Authors. Advanced Materials Technologies published by Wiley-VCH GmbH

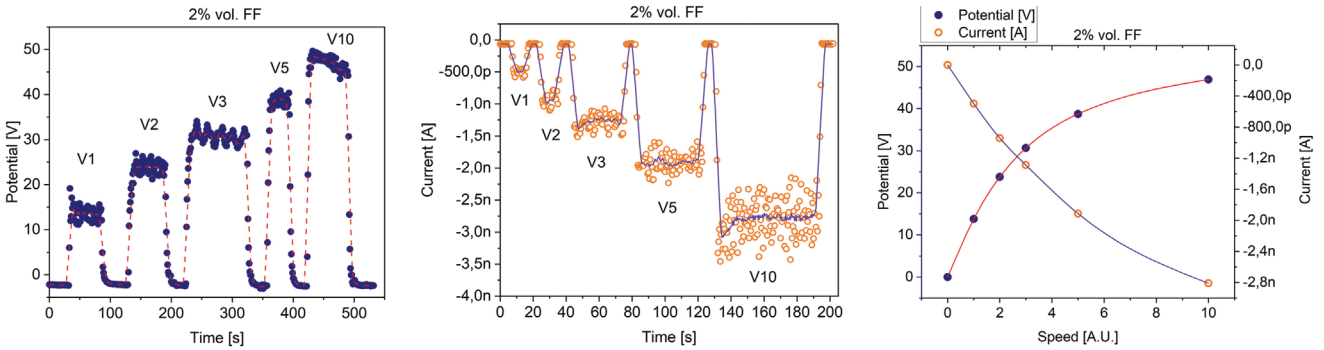


Figure 2. Recorded potential (left) and current (center) on the capacitive electrode versus time and speed (right).

temperature (RT). As expected, increasing the fluid velocity a more sudden temperature drop occurs and then **Figure 3** shows a gradual increase in the recorded potentials and currents. With respect to the RT condition, the electrical outputs are clearly higher, confirming that a pyroelectric phenomenon is taking place. Considering that at RT the max potential recorded is about 25 V it is evident how the capacitive electrode is more performing when exploiting triboelectricity, while the measured currents up to 22 nA suggest that the resistive electrode is a better option for collecting charges generated by the pyroelectric effect.

2.2. Estimate of Pyroelectric Coefficient

To quantify the pyroelectric generation occurring in the FF we estimated the pyroelectric coefficient p_I of the same. To do so, we relied on the electric contact method discussed.[23] This static method is particularly convenient since it provides a compact formula that allows expressing this coefficient as:

$$p_I = \frac{I_p \cdot C_M}{A_e \cdot F_h} \tag{1}$$

where I_p represents the measured pyroelectric current, A_e the effective electrode area, C_m is the heat capacity of the solid fraction and $F_h = -k\frac{dT}{dx}$ with k thermal conductivity the heat flux crossing the pipe area. However, since neither uniform/spatially varying viscous stresses nor electric fields are taken into account, this does not allow the evaluation of the other components of p_I.

Particular attention must be paid to A_e which indicates that the area under consideration is not represented by the whole area of the electrode but rather the one where the particles release the accumulated charge. Therefore, we need to quantify the particle deformation when in contact with the electrode (see **Figure 4**, representing the case for a rigid particle). In our case, the magnetite NPs are covered by a monolayer of compressible oleic acid (OA) which absorbs part of the impact. Thus, knowing the particles velocities in proximity to the electrode, we can estimate the impulsive force and account for the deformation of the OA. At this point, the remaining force will be the one actually deforming the particles. To do so, we assume that the OA molecules are completely deformed by the impact and that a typical OA chain length is l_{oa} = 2 nm and width is w_{oa} = 0.5 nm. We know the compression modulus E_{oa} of OA which gives the compression force F_{oa}, once multiplied for the contact area.[24]

The residual force F_r will simply be the difference between the impulsive force F_i and F_{oa}. The radius a of the deformed region can be expressed as:

$$a = R\sqrt{\frac{\omega}{R}}\left(\frac{\omega}{1.9\omega_c}\right)^{\frac{B}{2}} \tag{2}$$

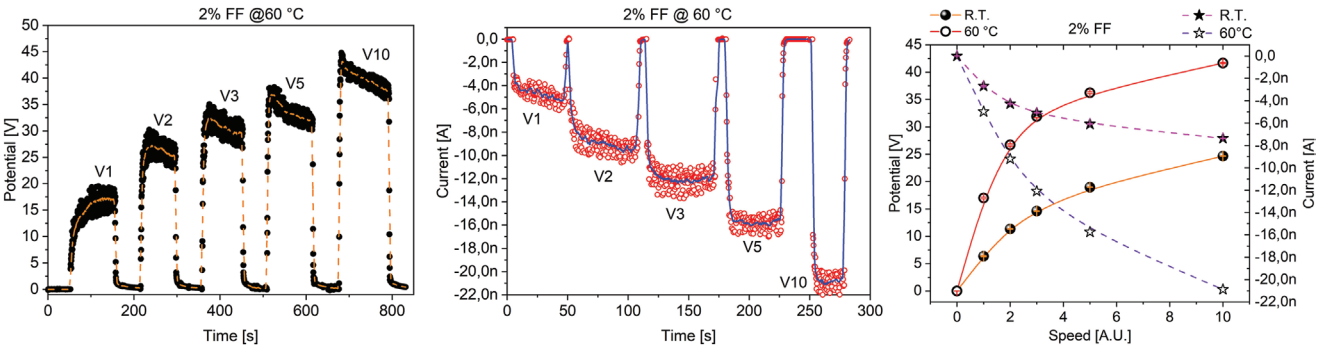


Figure 3. Recorded potential (left) and current (center) on the resistive electrode when the colloid is heated up to 60 °C. Comparison (right) between the two situations.

© 2022 The Authors. Advanced Materials Technologies published by Wiley-VCH GmbH

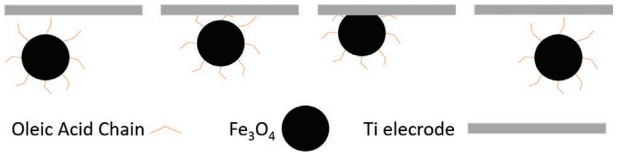


Figure 4. Representation of the dynamics of a magnetite nanoparticle (NP, black sphere) functionalized with oleic acid (OA; orange segments) hitting a Ti electrode.

where the relation with the residual force is accounted for in the indentation factor ω:

$$\omega = \frac{F_r}{2\pi \cdot E \cdot R \cdot \omega_c} \tag{3}$$

where R indicates the particles radius, $\omega_c = \left(\frac{\pi c S_y}{2E}\right)^2 \times R$ the critical indentation and B a material parameter that accounts for the relation among the yield strength S_y and the young modulus E according to:

$$B = 0.14 \exp\left[23\left(\frac{S_y}{E}\right)\right] \tag{4}$$

Notice that in the computation of the deformation area the average particle velocity has been taken into account, since the number of particles hitting the surface per unit of time changes according to the flow rate, modifying the contact area with the electrode. The results of this analysis lead to a pyroelectric coefficient of 25.2 ± 0.3 μCm^{-2} K^{-1} for the slow flow rates, until 0.44 mm s^{-1}, while we observe a decrease at 2.2 mm s^{-1} flow rate giving 15.0 ± 0.2 μCm^{-2} K^{-1}. A visual representation of extrapolated data is provided in **Figure 5**. This can be explained observing the dynamic of the fluid flowing in the tube: because of the drag force exerted onto the pipe's walls, the motion of the fluid is expected to be Poiseuille-like. Consequently, increasing the flow rate, FF drag force increases provoking a slowdown of the fluid close to the pipe walls and leads to an overestimate in our analysis of the number of particles able to reach the electrode.

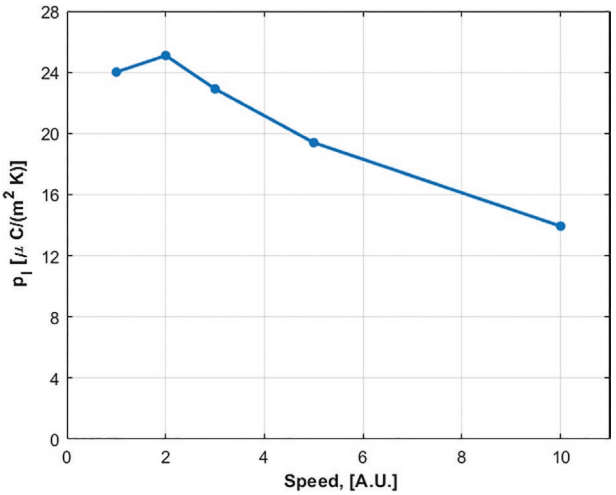


Figure 5. Calculated pyroelectric coefficient versus the flow speed of the ferrofluid (FF).

2.3. Electronic Conductivity Analysis

To verify that recorded voltages and currents with each setup are effectively produced from the energy conversion processes and the equipment employed for the measurements does not induce any bias, we analyzed the electronic conductivity at RT of the FF at different concentrations, conducting a polarization tests and an impedance spectrum analysis. From **Figure 6**, it is evident that that the FF behaves as a quasi-ideal capacitor at all concentrations tested (0.5%, 1%, 2%, 4%, 6%, and 8% vol.) with very high values of electric resistance (colored boxes in Figure 6), highlighting the high resistive behavior of FF, slightly decreasing with increasing concentrations. It is clear that the resistance (real part of impedance) is higher for smaller concentrations, and the reactance (imaginary part), is higher too. Therefore we justify the choice of focusing on the higher FF concentration spectrum (>2%).

2.4. Model of Equivalent Circuit

Finally, an equivalent circuit has been modeled on the inductive electrode data. We provided an impedance spectroscopy analysis

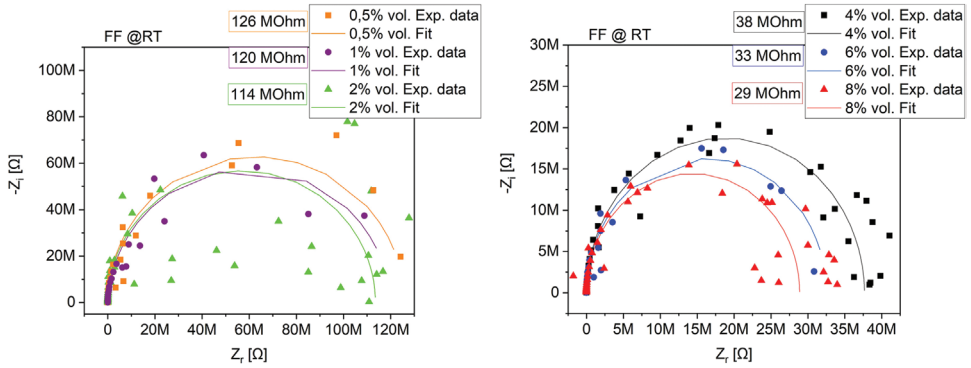


Figure 6. Impedance spectrum analysis at room temperature (RT) of ferrofluid (FF) at different concentrations. Intercepts with *x*-axis represent the values of electronic resistance of the material and are indicated in the boxes along with FF solid volumes.

© 2022 The Authors. Advanced Materials Technologies published by Wiley-VCH GmbH

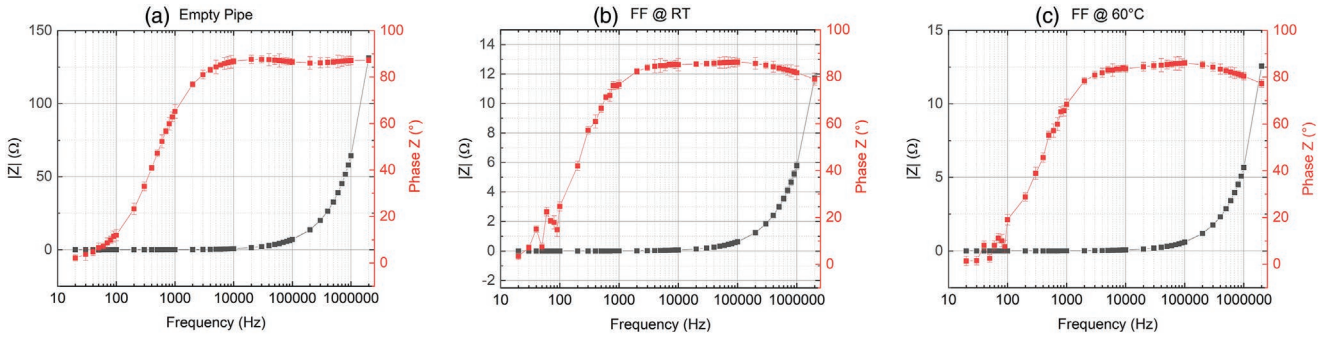


Figure 7. Bode diagram of impedance associated to: a) empty pipe, b) pipe filled with 2% vol. ferrofluid (FF) at room temperature (RT), and c) pipe filled with 2% vol. FF at 60 °C. Modulus is highlighted in black, phase in red.

(Agilent E4980A Precision LCR Meter) on three different samples: empty pipe, 2% vol. FF at RT and heated at 60 °C, both in static condition (v_FF = 0 m s^{-1}) and in motion. Statistical analysis was performed on three different measurements for each sample.

At first, we analyzed the electrode impedance contribution considering the spectroscopy response: it is possible to observe from the Bode Diagram (**Figure 7**) that the modulus is described by an increasing monotone function, with a diphase of 90°. Thus, the inductive electrode can be modeled as a resistance that represents the resistive material properties of the wire used as electrode, in series with an inductance (**Figure 8**), which represents the solenoidal arrangement of the inductive electrode:

$$Z_{\text{Empty}} = R_{\text{Wire}} + j\omega L_{\text{Solenoid}} \tag{5}$$

The equivalent resistance R_{Wire} can be evaluated considering $Z_{\text{Empty}}(\omega \to 0)$, while the inductance is represented by the slope of impedance modulus at high frequencies $Z_{\text{Empty}}(\omega \to +\infty)$: $R_{\text{Wire}} = 34 \pm 2$ mΩ and $L_{\text{Solenoid}} = 11.48 \pm 0.34$ µH (mean value and standard deviation).

Since the electrode can be modeled as a series of two impedances, it was possible to highlight the FF contribution subtracting the calibration values of impedance to the measurement performed with a full pipe condition. With this experimental setup, we were able to measure with statistical relevance (paired *t*-test $p > 0.01$) the variation of internal magnetization due to the effect of temperature. Also in this case, all the physical parameters involved in FF behavior are represented by means of a series inductance. The relative evaluation of inductance is evaluated as before considering the slope of impedance modulus at high frequencies: $L_{\text{Ferrofluid}}(T = 25\ °C) = 1.13 \pm 0.01$ µH and $L_{\text{Ferrofluid}}(T = 60\ °C) = 1.07 \pm 0.01$ µH.

Note that the presence of a superparamagnetic fluid subject to an external permanent magnetic field will increase the whole inductance due to an increase in relative magnetic permittivity, and increasing the fluid temperature there will be a reduction of the FF inductance due to demagnetization effects.

3. Conclusions

In conclusion, results suggest that FFs behave as both a triboelectric and a pyroelectric material. While the capacitive electrode is more efficient for accumulating charges developed by triboelectricity up to 48 V, the resistive one is essential to collect, in direct contact with the FF, the charges displaced by pyroelectric phenomena up to 22 nA. In comparison, induction effects have better performances for extracting currents of three orders of magnitude higher while the induced electromotive force is of six orders of magnitude lower. FF magnetic properties are moreover appealing especially in robotic applications when they can be exploited for controlling the fluid dynamics in order to optimize energetic system but also for developing mobility system, similarly to what already happens in biomedical nano/micro robotics.

4. Experimental Section

In order to characterize the energy harvesting capabilities of the FF, we set the motion of EMG 901 oil-based FF (Ferrotec) through a fluorinated ethylene propylene (FEP) pipe, chosen because of its triboelectric properties[18] which define it as a negative element in the triboelectric series.[19,20] Since hydrocarbon oils tend to charge positively in presence of electronegative elements, FEP is the perfect candidate for characterizing the triboelectric effect of the FFs.[21] A peristaltic pump (Ismatec MCP) was used to generate a tunable motion through a FEP pipe with an inner diameter (ID) and outer diameter (OD) of 10 and 12 mm, respectively. The Ismatec MCP provides a rotor system that allows pipes with a maximum internal diameter of 3.2 mm. This permits to generate at the maximum rotational

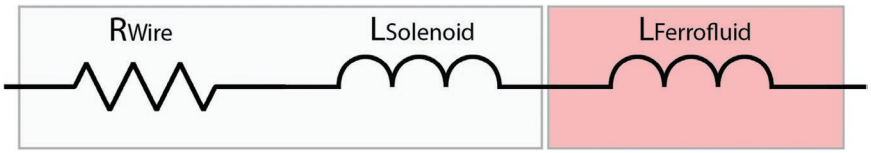


Figure 8. Equivalent circuit model of ferrofluid (FF) using inductive electrode. The gray part represents the electrode contribute by means of internal wire resistance and geometrical solenoidal arrangement. The light red describes the physical parameters associated to static FF, as function of concentration, temperature, and external permanent magnetic field.

© 2022 The Authors. Advanced Materials Technologies published by Wiley-VCH GmbH

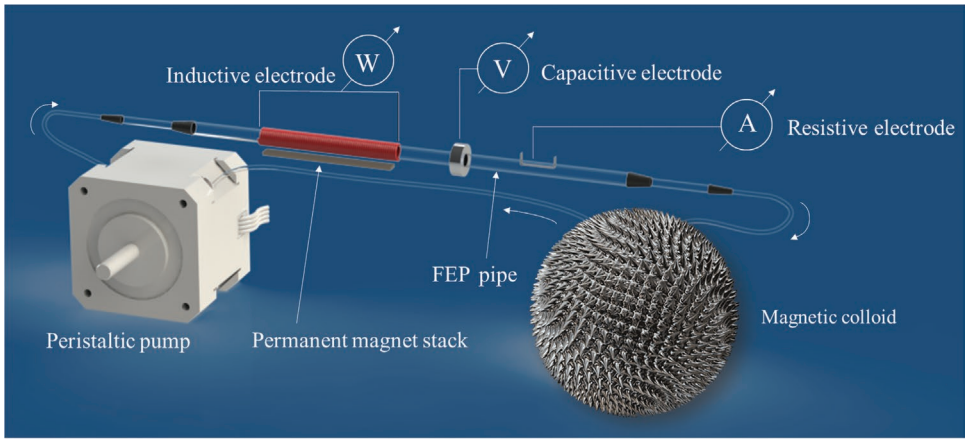


Figure 9. Rendering of the experiment.

speed a flow rate of 100 mL min^{-1} for each channel, up to eight channels. A silicone pipe with internal and external diameters of 3.2 and 4 mm, respectively, was coupled with the rotor system of the peristaltic pump; then, a series of intermediate pipes and adapters allowed connecting the testing pipe. The accumulation system consists of an aluminum capacitive electrode (ID = 12 mm, OD = 28 mm, length = 9 mm) anchored externally to the FEP pipe in single electrode mode (SEM) configuration,[22] in order to collect the charges developed by triboelectricity in the pipe. V_{OC} and I_{SC} measurements were conducted respectively by means of SourceMeter-Keithley 2635A and Keithley 4200-SCS coupled with a Keithley 4225-RPM Remote Amplifier (Tektronix). On the other hand, to explore the FF's ability of inducing electromotive forces we installed an oxygen free copper (OFC) inductive electrode wrapping the FEP pipe (100 mm long and 2.5 mm in diameter) with 40 windings around the pipe, coupled with a stack of 7 $AlNiCo_5$ permanent magnets with the aim of magnetizing the colloid locally. The coil was connected to the SourceMeter-Keithley 2635A to perform an V_{OC} measurement, to the Semiconductor characterization system Keithley 4200-SCS coupled with a low-noise amplifier Keithley 4225-RPM for measuring the I_{SC}, and to the impedancemeter Agilent E4980A for an impedence analysis. Finally, to evaluate the pyroelectric phenomena occurring on the Fe_3O_4 NPs, we immersed a titanium resistive electrode (SigmaAldrich, purity 99.98%, width = 5 mm, length = 30 mm, thickness = 0.2 mm, surface area = 300 mm^2), in the pipe to harvest the charges generated in the fluid because of the temperature gradient. As reference electrode an identical electrode was immersed in the reservoir. V_{OC} and I_{SC} measurements were conducted, respectively, by means of two SourceMeter-Keithley 2635A. All the instruments were connected to a PC with LabVIEW 2019 software (National Instruments). **Figure 9** shows an overview of the global setup, where we represented the three different electrodes together with the peristaltic pump, the heater, the FEP pipe, and the FF reservoir. We measured the energy harvesting response as a function of a broad spectrum of fluid velocities, up to 3 cm s^{-1}, while applying two heating conditions, RT and heating at 60 °C, with the aim of analyzing the effect of different heat fluxes and thermofluid dynamic conditions on the colloid.

Acknowledgements

Open access Funding provided by Istituto Italiano di Tecnologia within the CRUI-CARE Agreement.

Conflict of Interest

The authors declare no conflict of interest.

Data Availability Statement

The data that support the findings of this study are available from the corresponding author upon reasonable request.

Keywords

colloids, energy harvesting, ferrofluids, pyroelectricity, thermoelectrics, triboelectricity

Received: January 23, 2022
Revised: April 5, 2022
Published online:

[1] N. Soin, *Magn. Nanostruct. Materials.* **2018**, 295.
[2] A. Chiolerio, E. Garofalo, M. Bevione, L. Cecchini, F. Mattiussi, *Energy Technol.* **2020**, *8*, 2000413.
[3] B. El Zein, *Adv. Rob. Autom.* **2013**, *2*, 1000113.
[4] M. Han, H. Wang, Y. Yang, C. Liang, W. Bai, Z. Yan, H. Li, Y. Xue, X. Wang, B. Akar, H. Zhao, H. Luan, J. Lim, I. Kandela, G A. Ameer, Y. Zhang, Y. Huang, J. A. Rogers, *Nat. Electron.* **2019**, *2*, 26.
[5] Y. Cha, S. Hong, *Smart Mater. Struct.* **2016**, *25*, 10LT01.
[6] D. Trivedi, C. D. Rahn, W. M. Kier, I. D. Walker, *Appl. Bionics Biomech.* **2008**, *5*, 520417.
[7] S. A. Katiyar, F. Iida, S. G. Nurzaman, *Int. Conf. Cybernetics and Intelligent Systems (CIS) and IEEE Conf. Robotics, Automation and Mechatronics (RAM)*, Bangkok **2019**, 475.
[8] H. Shahsavan, A. Aghakhani, H. Zeng, Y. Guo, Z S. Davidson, A. Priimagi, M. Sitti, *Proc. Natl. Acad. Sci. U. S. A.* **2020**, *117*, 5125.
[9] A. Chiolerio, M B. Quadrelli, *Adv. Sci.* **2017**, *4*, 1700036.
[10] A. Chiolerio, M B. Quadrelli, *Energy Technol.* **2019**, *7*, 1800580.
[11] E. Garofalo, L. Cecchini, M. Bevione, A. Chiolerio, *Nanomaterials* **2020**, *10*, 1181.
[12] M. Bevione, E. Garofalo, L. Cecchini, A. Chiolerio, *MRS Energy & Sustainability*, Vol. *7*, Cambridge University Press, Cambridge **2020**.
[13] A. Bozhko, G. Putin, *Microgravity Sci. Technol.* **2009**, *21*, 89.
[14] M. Yang, R. O'Handley, *Excerpt from the Proc. COMSOL Conf*, Boston **2010**.
[15] J. G. Monroe, E. S. Vasquez, Z. S. Aspin, K. B. Walters, M. J. Berg, S. M. Thompson, *Appl. Phys. Lett.* **2015**, *106*, 263901.

© 2022 The Authors. Advanced Materials Technologies published by Wiley-VCH GmbH

[16] A. Chiolerio, E. Garofalo, F. Mattiussi, M. Crepaldi, G. Fortunato, M. Iovieno, *Appl. Energy* **2020**, *277*, 115591.
[17] P. Dubois, M. Bergé, *Contemp. Phys.* **1984**, *25*, 535.
[18] Z. L. Wang, L. Lin, J. Chen, S. Niu, Y. Zi, *Triboelectric Nanogenerators*, Springer International Publishing, Berlin **2016**.
[19] M. Ko, *Nano Energy* **2018**, *53*, 37.
[20] M. Sakaguchi, Y. Miwa, S. Hara, Y. Sugino, K. Yamamoto, S. Shimada, *J. Electrostat.* **2004**, *62*, 35.
[21] A. K. T. Assis, *The Experimental and Historical Foundations of Electricity*, Vol. *2*, Apeiron, Montreal **2018**.
[22] H. Y. Park, H. K. Kim, Y. H. Hwang, D. M. Shin, *J. Korean Phys. Soc.* **2018**, *72*, 499.
[23] S. Jachalke, E. Mehner, H. Stöcker, J. Hanzig, M. Sonntag, T. Weigel, T. Leisegang, D. C. Meyer, *Appl. Phys. Rev.* **2017**, *4*, 021303.
[24] M. Kepczynski, J. Lewandowska, K. Witkowska, S. Kędracka-Krok, V. Mistrikova, J. Bednar, P. Wydro, M. Nowakowska, *Chem. Phys. Lipids* **2011**, *164*, 359.
[25] S. S. Wadwalkar, R. L. Jackson, L. Kogut, *Proc. Inst. Mech. Eng., Part J* **2010**, *224*, 1091.

© 2022 The Authors. Advanced Materials Technologies published by Wiley-VCH GmbH